Modification of hydroxyapatite surface properties by electron irradiation

Guillaume Bai, Jean-Christophe Hornez, Ulrich Maschke, Philippe Supiot, Etienne Bres

Modification of hydroxyapatite surface properties by electron irradiation

Guillaume BAI

Unité des Matériaux et Transformations, Université de Lille, CNRS, INRA, UMR 8207, F-59000 Lille, France.

guillaume.bai@univ-lille.fr

Jean-Christophe HORNEZ

Laboratoire des Matériaux Céramiques et Procédés Associés (LMCPA), UPHF- Université Polytechnique Hauts-de-France, 59600 Maubeuge, France.

jean-christophe.hornez@uphf.fr

Ulrich MASCHKE

Unité des Matériaux et Transformations, Université de Lille, CNRS, INRA, UMR 8207, F-59000 Lille, France.

ulrich.maschke@univ-lille.fr

Phillipe SUPIOT

Institut d'Électronique de Microélectronique et de Nanotechnologie (IEMN), Université de Lille, CNRS UMR 8520, 59650 Villeneuve d'Ascq, France.

phillipe.supiot@univ-lille.fr

Etienne BRÈS

Unité des Matériaux et Transformations, Université de Lille, CNRS, INRA, UMR 8207, F-59000 Lille, France.

etienne.bres@univ-lille.fr

Abstract

In the present work, the modification of wetting properties of EB irradiated HA ceramics are studied under air and N_2 gas atmospheres. We show a noticeable increase of the hydrophily of electron irradiated HA ceramics in an air atmosphere and a lesser increase when the samples are irradiated in an N_2 atmosphere, such a phenomenon is correlated to a modification of grain morphology obtained under the two atmospheres. With a progressive water saturation of the ceramics, the wetting angles increase progressively until they reach a plateau value different from each set of samples (irradiated under air, irradiated under N_2 atmosphere and pristine). Profilometry, SEM/EDX, XRD and Raman spectrometry analysis do not show differences between irradiated and pristine samples which indicates that the EB irradiation modifies the surface chemical elements related to the surface wetting properties and not those analysed by the above techniques.

Keywords: Hydroxyapatite; Electron irradiation; surface modification, surface fonctionnalisation, surface wettability.

1. Introduction

Hydroxyapatite (HAP, $Ca_{10}(PO_4)_6(OH)_2$, $P6_3/m$) has a close similarity to the inorganic components of teeth and bones. Due to its biocompatibility to living tissues, HAP is currently used as a ceramic [1,2], a coating or as vector nanoparticles for biomedical applications [3].

As an ionic material HAP show specific surface properties [4,5] that favours the accommodation of a large variety of molecules that can be used for inducing specific medical responses [6].

A further consequence of the HAP ionic nature is its specific behavior when subjected to electron irradiation in the electron microscope as a function of different beam characteristics: accelerating voltage, fluence and fluence rate, induced temperature rise…

1.1 Effect of electron beam irradiation on HAP

1.1.1 Radiation damage

Accelerating voltage: ballistic or ionization damage?

Recent observations by Eddisford *et al.* [7] show that the damage is more important as the voltage decreases which indicates that the damage process is dominated by radiolysis, which would explain the breaking of the P-O covalent bonds and the displacement of the P^{5+} and O^{2-} ions outside the apatite bulk. In addition to this, the formation of dislocation lines and dislocation loops was observed at very high voltages, 2 mV, during the observation of HAP crystals [8].

Effect of the beam fluence and fluence rate on HAP

A significant dependence of the extent and type of damage of HA at a given fluences or fluence rates has been shown by Eddisford *et al.* and Reyes-Gasga *et al.* [7,9]. Nanovoids are formed on the faces of the crystals at fluence rates below 1.6 A cm^{-2} [10,11], these voids can be subsequently filled after prolonged irradiation [12]. This shows a structural destruction without material loss. Above 1.6 A cm^{-2} the bulk of the crystals become amorphous while CaO particles form at the surface of the crystals. Eddisford et al., Meldrum et al. and Brès et al. [7,11 and 12] have reported that a recovery process becomes appreciable above a fluence rate of about 80 Acm^{-2}. They also report that fluence seems to have no influence on damage below a value of about 1600 Ccm^{-2} with no reduction of damage with sample cooling. Lastly, a transformation of the apatite hexagonal

phase (space group: $P6_3/m$) into a monoclinic phase has been suggested [7]. TEM-Electron energy loss spectrometry of HA at 150kV have shown no mass loss for fluence rates 160 A cm^{-2} and dose rate= 70 Acm^{-2} and no formation of CaO [13].

Beam induced temperature rise at the sample

The temperature at a material irradiated by the electron beam inside an electron microscope is difficult to assess. It not only depends on the experimental parameters but also on the thermal diffusivity of the material itself [14]. Concerning calcium phosphate, indication on the temperature at the material level can be given by the existence or the absence of chemical reactions. In situ transformation of octacalcium phosphate (OCP) into hydroxyapatite does not show the presence of additional phase [15]. Such a transformation has been observed *in situ* has shown the existence of a transient phase in the transformation of calcium deficient apatite during TEM observation [16].

Electron beam induced properties modifications

Effects of electron irradiation on HA solubility

Recently, electron irradiation at very high energy 3-10 MeV (3.42, 10.27, 20.54 Gy, irradiation times: 5h, 15h, 30h) has been shown to increase HA solubility through the creation of crystal defects [17].

Effect of electron irradiation on HA surface hydrophily

Electron and UV irradiation have been used for modifying the surface of HA solid surface [18,19], a decrease of wettability induced by a low energy irradiation of the solids has been shown by Aronov *et al.* [20,21]. The phenomenon being reversible when UV radiation is applied. A method for tuning the wettability properties of HA ceramics from 10° to 100° with an accuracy of +/-3° using very low energy and fluence has been described (electron energy = 100 eV, fluence rate = 100 $nAcm^{-2}$, exposure time = 0-3000 s, vacuum = 10^{-7} Torr). This enabled the differential binding of biological materials with different surface properties, such as bovine serum albumin (BSA) and deoxyribonucleic acid (DNA) [22], controlling the bacterial adhesion on HA-titanium implants [23]. Lately, we have shown a wettability modification of human tooth surfaces by water and UV and electron-beam radiation [24].

2. Materials and methods

2.1. Processing of the pellets

Hydroxyapatite Calcium phosphate powders were precipitated from a Calcium Nitrate precursor $Ca(NO_3)_2$-$4H_2O$ (Brenntag, France) and an diammonium Phosphate precursor $(NH_4)_2HPO_4$ (Carlo Erba, France) by aqueous precipitation[1-2] with the control of parameters such as: temperature, solution pH, stirring, For Hydroxyapatite (HAP) powders syntheses, temperatures were set at 50°C and pH at 8.0. The initial Ca/P molar ratios are 1.67 with an aging time of 20 hours. The precipitate was filtrated on a filtration set-up (*i. e.* Buchner funnel) and dried in an oven. After this, the solution was filtered, and the precipitate was dried at 70°C. Powders were then calcined in order to reduce the grain specific surface in order to improve slip casting. Then to make a slip, grains were calcined to become bigger and putted in solution to be crushed. This will lead to eliminate clusters induce by calcination. The powders whereas then again filtrated and dried. ground 48 hours to break up agglomerates formed during the thermal treatment and reduce the powder to its ultimate particle size. This grinding step was carried out by ball milling using a HDPE milling jar and yttrium stabilized zirconia grinding media. The slip was created by auditioning water and adjuvants to the powder. The slip was then shaped into pellets in plaster moulds. The HA slurries were prepared in water with a powder concentration of 65 wt. %. Slurry defloculation is obtained by adding polyacrylate ammonium (Darvan C, R. T. Vanderbilt Co.) with 1.5 wt % of HA powder. Slurry dispersion was ensured by a ball milling for 1 hour. Slurries were casted into a cylindrical plaster mould (Φ = 15 mm, h = 5 mm). And finally, pellets were sintered at 1250 °C in air atmosphere. The heating and cooling rates were 5°C.min^{-1} and dwell time was fixed to 3 hours.

Characterization of the pellets before irradiation

Samples were characterized by Fourier Transform Infrared spectrometry (FTIR), X-ray diffractometry (XRD), Scanning Electron Microscopy (SEM), energy dispersive X-ray spectrometry (EDX) and Time of flight Secondary Ions Mass Spectroscopy (Tof-SIMS) Profilometry.

Polishing the pellets

Pellets were polished using #800, #1200 and #4000 SiC Struers papers on a manual Struers Rotopol-22 polishing machine.

Conservation of the pellets

After polishing, all samples were washed in an ultrasonic bath (S30 H Elmasonic) in a solution of tetrahydrofuran (Sigma-Aldrich®) for 15 min at 30°C. The pellets were then placed in a vacuum desiccator until used.

2.2. Electron irradiation (EB)

2.2.1. Description of the machine

The device use to conduct electron irradiation is a COMET-Beam Sources equipment (COMET Technology Model EBLab 180/210, Switzerland). It's composed of an electron beam that irradiates samples and a carriage that moves during exposure. Electrons are accelerated by an electric field in vacuum through a titanium window. The carriage speed, the accelerating voltage, the beam intensity and the distance between the titanium window and the surface of the sample are controlled.

2.2.2. Irradiation conditions

The EB radiation conditions were: accelerating voltage 150 kV, carriage speed 3 m/min, air gap 10 mm, beam current 12,5 mA, duration of irradiation 0.8 s for a surface dose around 460 kGy (~2.72×10^{-2} mA.cm^{-2}). This correspond to an irradiation time of 0.8 s.

2.2.3. Gas atmospheres

EB irradiations were performed both in inert (N_2, 2 SLPM (Standard Litre per Minute)) and ambient air gas atmospheres.

2.3. Contact angle measurements

Distilled water sessile 2 µL drops were deposited on the sample surface by a syringe and the contact angle were measured using a KRUSS Drop Shape Analyser 100. For this equipment, the standard deviation for the contact angle measurement is ±5°. Optical inspection of the drops was performed by a camera device and digital imaging techniques. The measurement of the contact angle was taken 10 s after the deposition of the drops, the estimated time of equilibrium to be reached. Two measurements were made for each drop, one from the left-hand side and one from the right-hand side of the drop. Average measurements were used for the graphs. After each measurement, the water drop was wiped with absorbent paper. The homogeneity of the sample surface was evaluated by 5 measures, one at the center and 4 at each quadrant of the pellet as shown on Figure

1. This step permitted to concentrate our measurements at location 1 as explain below. In addition, measurements were carried out at regular time intervals at location 1. The results are present as a function of time. There is a 15s time interval between two measurements, corresponding to the necessary time of the stabilisation and the sweeping of the pellet surface with absorbent paper.

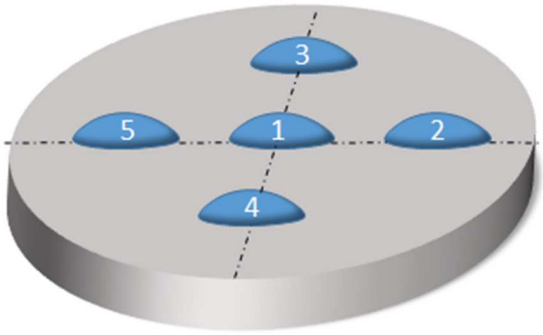

Figure 1. Locations of the drops on pellets for the contact angle measurements.

2.4. Profilometry

Profilometry data were recorded using an Alpha-Step IQ Surface Profiler. The roughness profile of all samples is the result of 3 measurements at different places on the surface. One on the centre and 2 others at different places. The scan length and the scan speed were 2 000 µm and 20 µm respectively. The average roughness Ra and the quadratic mean roughness Rq are the two main values mentioned.

2.5. XRD analysis

XRD (X ray diffractometry) data were recorded by using a Bruker AXS D8 Advance diffractometer at room temperature in a Bragg-Brentano geometry. Data were collected using the CuK_α line in a 2θ range from 10 to 60° with a step size of 0.02° and 0.5 s counting time per step.

2.6. SEM/EDX analysis

The samples were examined in a JEOL JSM-7800F LV scanning electron microscope (SEM) at 10 kV equipped with an electron dispersion X ray spectrometry (EDX) detector (OXFORD INSTRUMENT X-Max^N). The samples were metallized by a of Chromium coating prior to examination

Samples were observed at different magnifications: x150, x1 200, x2 500, x5 000 and x15 000 on at least 3 different areas. In some specific cases, samples were examined at: x10 000, x20 000 and x30 000 with a diminution of the accelerated tension to 5 kV to improve the sharpness of the images. And for all those magnifications, backscattered electrons and secondary electrons images were taken.

Chemical composition variations were investigated using energy-dispersive X-ray spectrometry combined with SEM at an accelerating voltage of 10 kV and at a 2 500x magnification.

2.7. Raman spectrometry analysis

Raman analyses were performed with a Labram confocal microspectrometer (Horiba Gr, Jobin Yvon, Lille, France). A helium-neon laser with a wavelength of 632.82 nm was used. The Raman spectrometer was coupled with an Olympus microscope (BX40). The 100x (Numerical aperture 0.80) objective was used to focus the laser light on the sample and to collect backscattering light. Spectra were recorded between 200 and 2 400 cm^{-1}. The spectral resolution was 4 cm^{-1}. One each sample, 5 spectra were recorded from different locations (according to figure 1). Each spectrum was the result of the average from two accumulations of 5 s. In some samples, multiple spectra were realised along the pellet diameter.

A water immersion lens was used for observing possible spectral modifications of the water saturated HA.

2.8. XPS (X-ray photoelectron spectrometry)

XPS experiments were carried out with a Kratos AXIS Ultra DLD instrument using a monochromatic Al Kα X-ray source (10 mA, 12 kV). O 1s, C 1s, Ca 2p, and P 2p high resolution spectra were obtained. All spectra were charge corrected to give the adventitious C 1s components (*i. e.* the thin carbonate material usually found on surfaces exposed to air) a binding energy of 284.8 eV. Spectra were analysed using Casa XPS software (version 2.3.16, Casa Software Ltd.). The spectra were quantified after a Shirley background subtraction.

3. Results

The effect of EB irradiation on the sample surface has been analysed in terms of: 1) wetting property (contact angle), 2) surface roughness (profilometry),3) topography and surface composition (SEM EDX), 4) fine structure analyses of the pristine and irradiated pellets (XRD, Raman and XP spectrometry).

3.1. Wetting property (contact angle)

The evolution contact angles vs time for repeated measurement/wipe processes is shown on Figure 2. All three sets of samples show similar behaviours, first "starting" angles are measured on the dry samples, then the contact angles increase up to stable "plateau" contact angles values. The measurements obtained from the three curves are shown on Table 1. Those values came from the average of 3 different samples in each case.

The most extreme values both for the starting contact angles and for the time to reach the plateau angle are obtained for the sample irradiated in air gas atmosphere, the values for the sample irradiated in N_2 gas atmosphere are in between the pristine and the sample irradiated in air.

This indicates that the modification of wetting property is obtained by a combination of EB irradiation and the chemical nature of the gas atmosphere surrounding the samples.

	Pristine sample	EB sample irradiated in air atmosphere	EB sample irradiated under N_2
Starting contact angle value	40±4°	19±4°	30±4°
Plateau angle value	85±5°	79±3°	77±3°
Time for reaching the plateau angle value	550 s	260 s	470 s
Amplitude between the starting angle value and the plateau	45±5°	60±4°	47±4°

Table 1. Starting contact angle value, plateau angle value, time for reaching the plateau angle value, amplitude between the starting contact and the plateau angle.

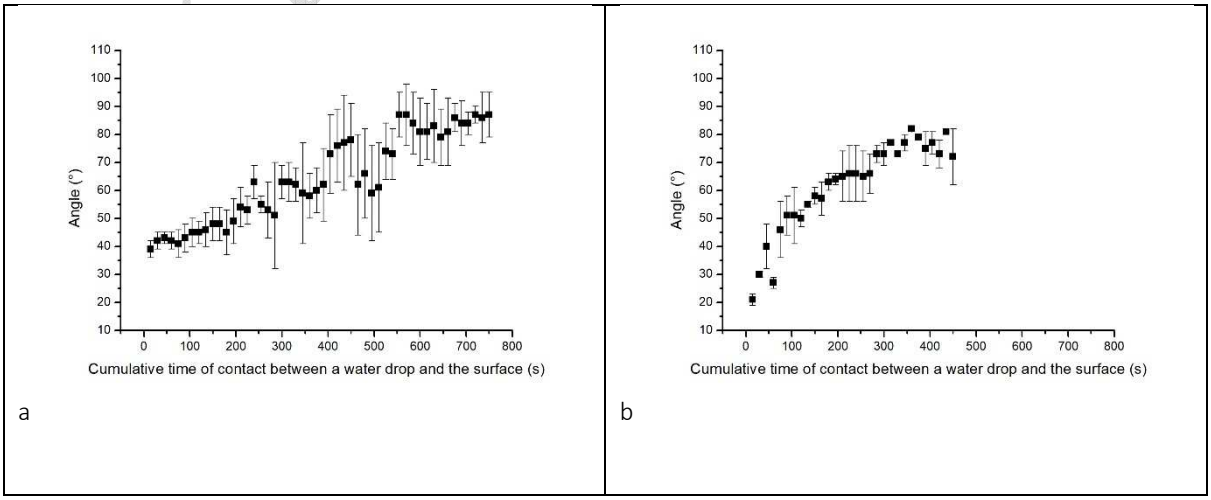

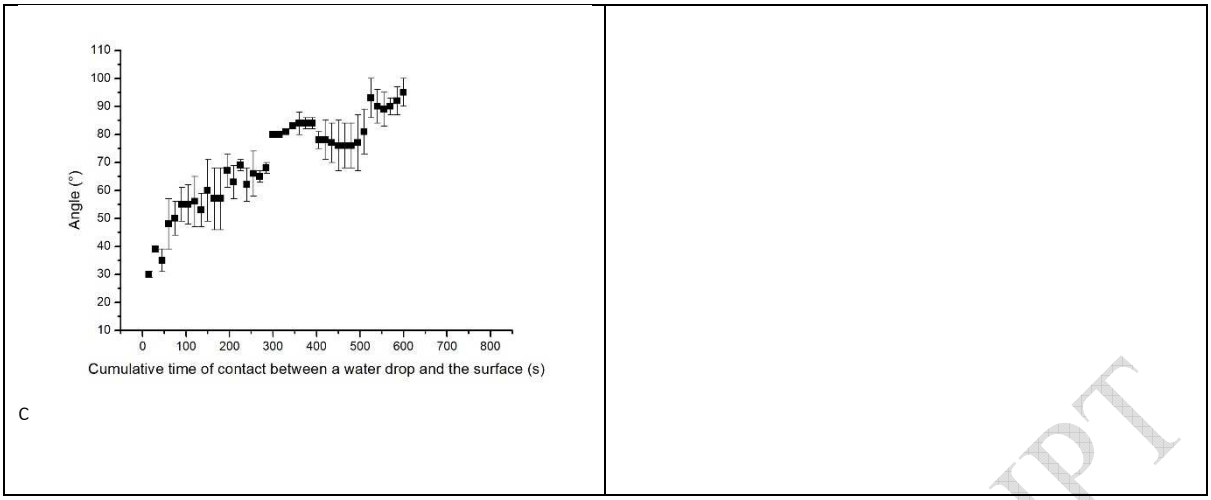

Figure 2. Evolution of contact angles for pristine samples (a), EB irradiated samples under air (b) and EB irradiated samples under N_2 atmospheres(c).

3.2. Surface roughness (Profilometry)

Roughness values are close between each sample with a low standard deviation. Non-significant differences were observed between the pristine and the irradiated samples, this indicates that the irradiation process does not influence the surface topography at the µm scale (Table 2).

	Pristine sample	EB irradiated sample under air	EB irradiated sample under N_2
Average Ra (µm)	0,13 ± 0.03	0,12 ± 0.04	0,14 ± 0.06
Average Rq (µm)	0,18 ± 0.04	0,18 ± 0.03	0,19 ± 0.04

Table 1. Average roughness Ra and quadratic mean roughness Rq for two pristine samples, two EB irradiated under air samples and two EB irradiated under N_2 samples.

3.3. SEM/EDX

The surfaces of pristine and irradiated samples show a variety of holes as we can see on image A1, B1 and C1 Figure 3. These holes are probably produced during polishing.

		A	B	C

Magnification x 150 / scare bar = 100 µm	1	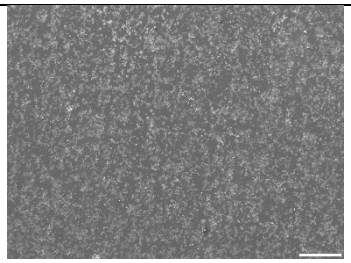	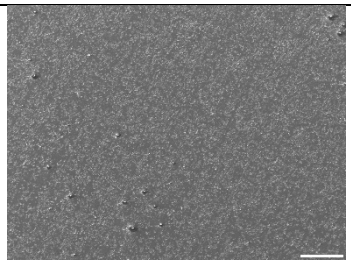	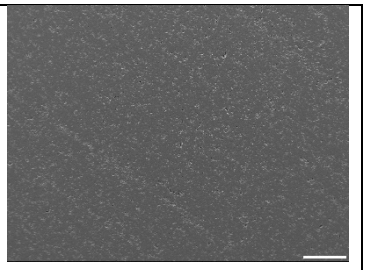
	2	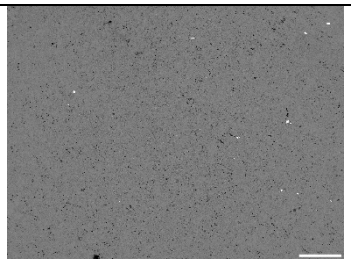	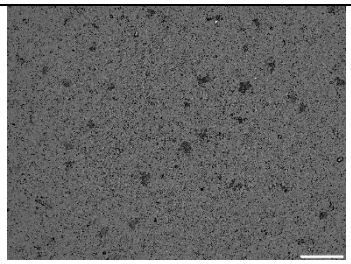	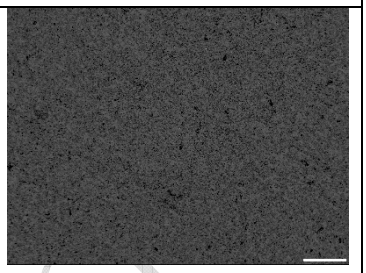
Magnification x 2 500 / scare bar = 10 µm	3	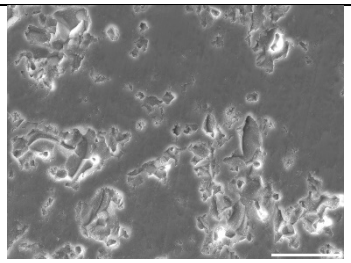	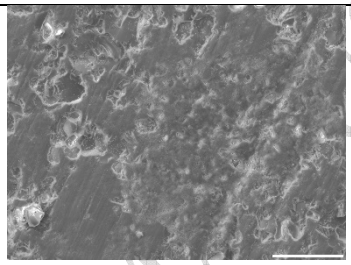	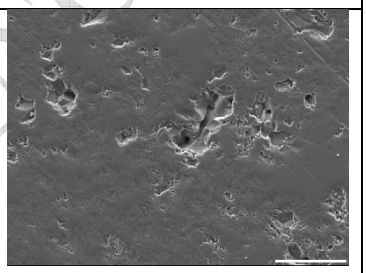
	4	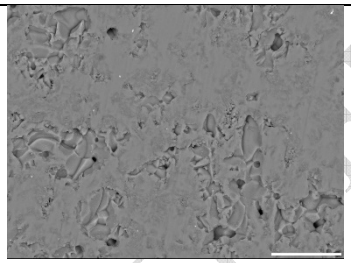	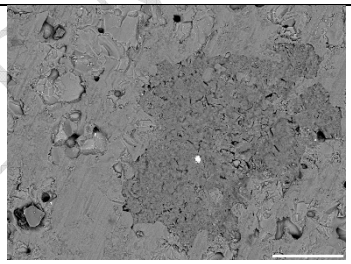	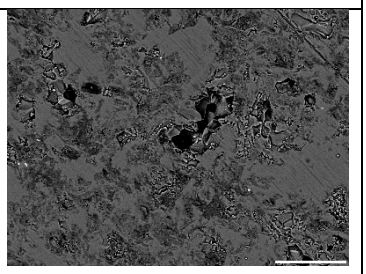
Magnification x 10 000 /	5	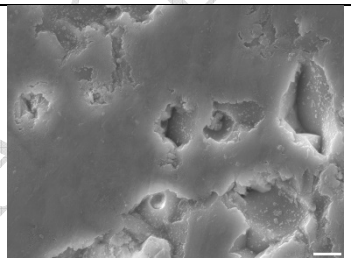	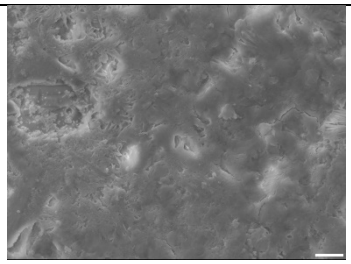	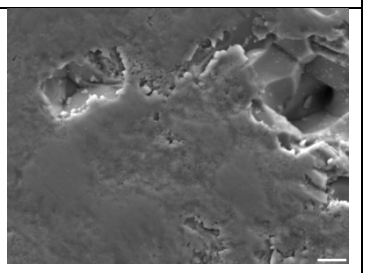

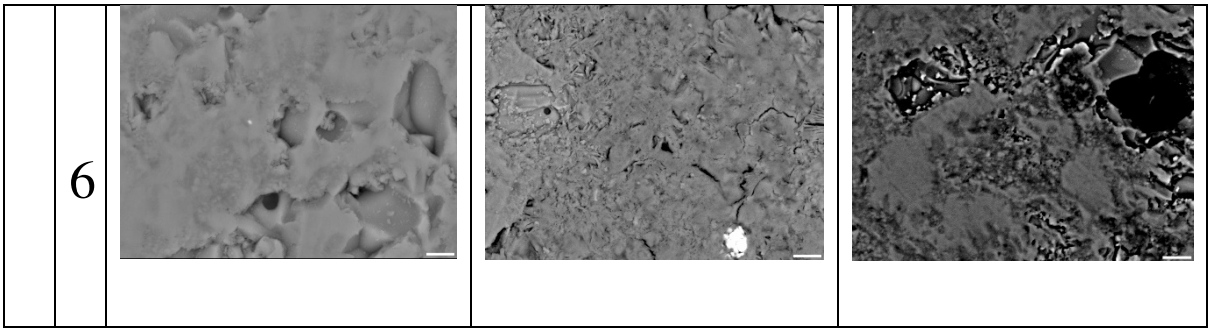

Figure 3. SEM images of pristine sample (A), irradiated sample under air (B) and irradiated sample under N_2 (C). Odd images were made with secondary electrons and even images with back scattered electrons.

3.3.1 Surface composition

Possible composition variations have been investigated using back scattered electron SEM and EDX spectrometry. All the useful images of a pristine sample, an irradiated sample under air and an irradiated sample under N_2 are present in figure 4 below.

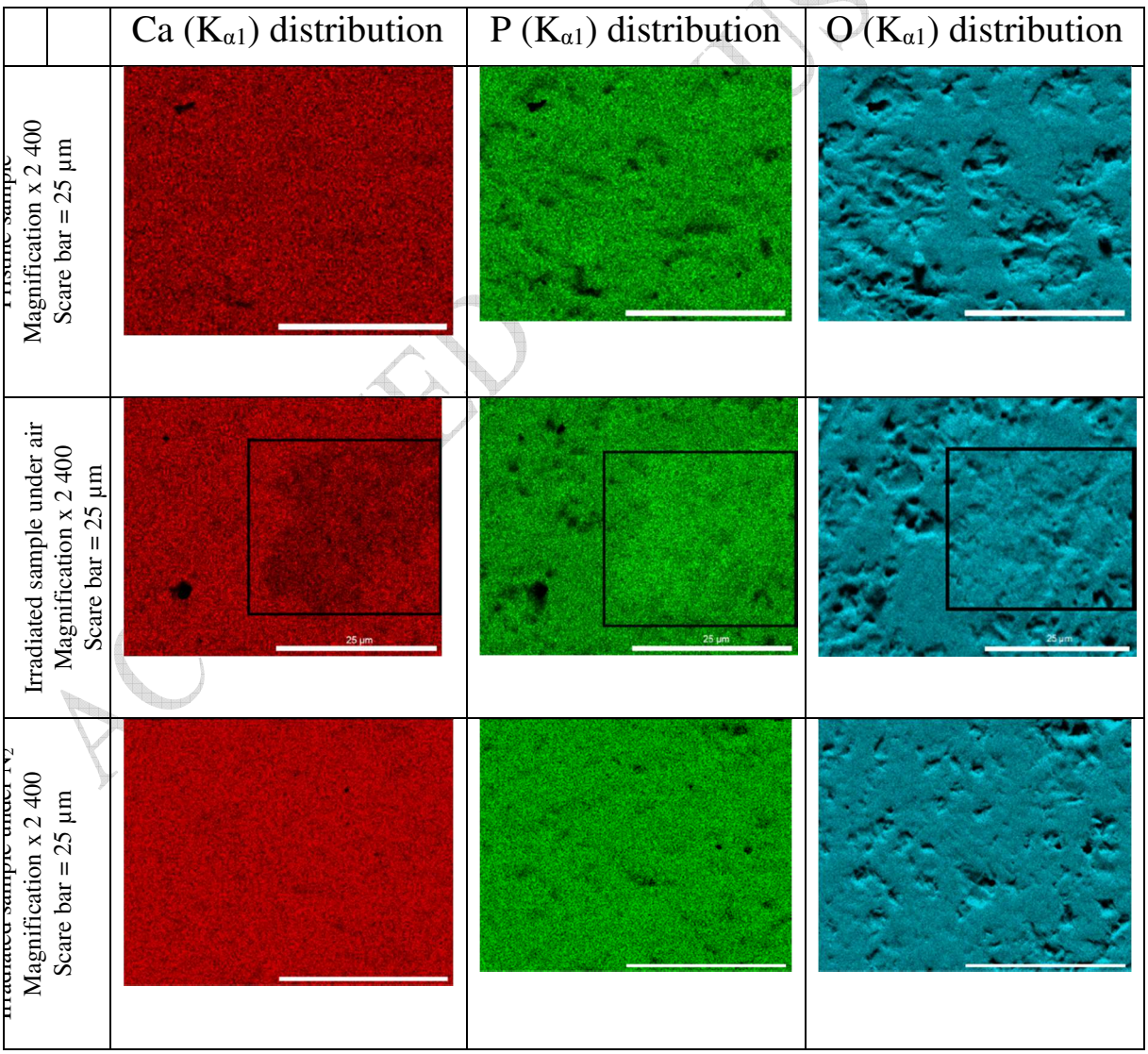

Figure 4. EDX images of a pristine sample, « darker » area (Figure 3. B4) of an irradiated sample under air and of an irradiated sample under N2.

3.3.1.1. EB irradiated sample in air atmosphere

Darker areas are observed of roughly 20µm diameter are observed (Figure 3, B2 and B4).

As controlled by EDX spectrometry (figure 4, Ca (Kα1) distribution), there appears to be a loss of Ca in these areas compared to the rest of the sample. Needle shape grains are observed on Figure 3, B6.

	Out of "darker" area	In the "darker" area
Ca (%at)	21	19
P (%at)	13	14

Table 3. Ca and P % composition obtained by EDX for an irradiated sample under air. Each result is the average of 3 measurements.

3.3.1.2. EB irradiated sample in N_2 atmosphere

Dark areas of smaller diameter (2 µm) similar to those observed on the air irradiated sample are seen (figure 3, C2 and C4). These areas are more uniformly distributed that those on the air irradiated sample.

3.4. XRD

No structure variation is observed between irradiated samples in gas atmosphere and pristine samples. The presence of amorphous or CaO phases are not observed (Figure 5).

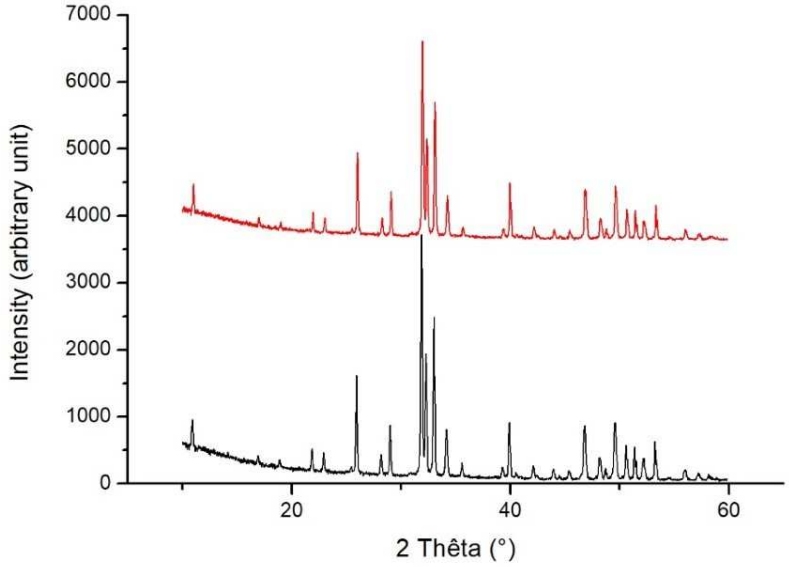

Figure 5. Diffractograms of the same sample at the pristine state (black) and at the irradiated under air state (red).

3.5. *Raman spectrometry*

No difference is observed between the pristine and the EB sample irradiated in air gas atmosphere (Figure 6).

Furthermore, spectra of pristine samples immersed from 1 minute to 3 hours (Figure 7) do not show any structure modification as no extra band is observed, only the intensities of existing bands are modified and this can't be allowed as a modification (due to water quantity modification during analysis).

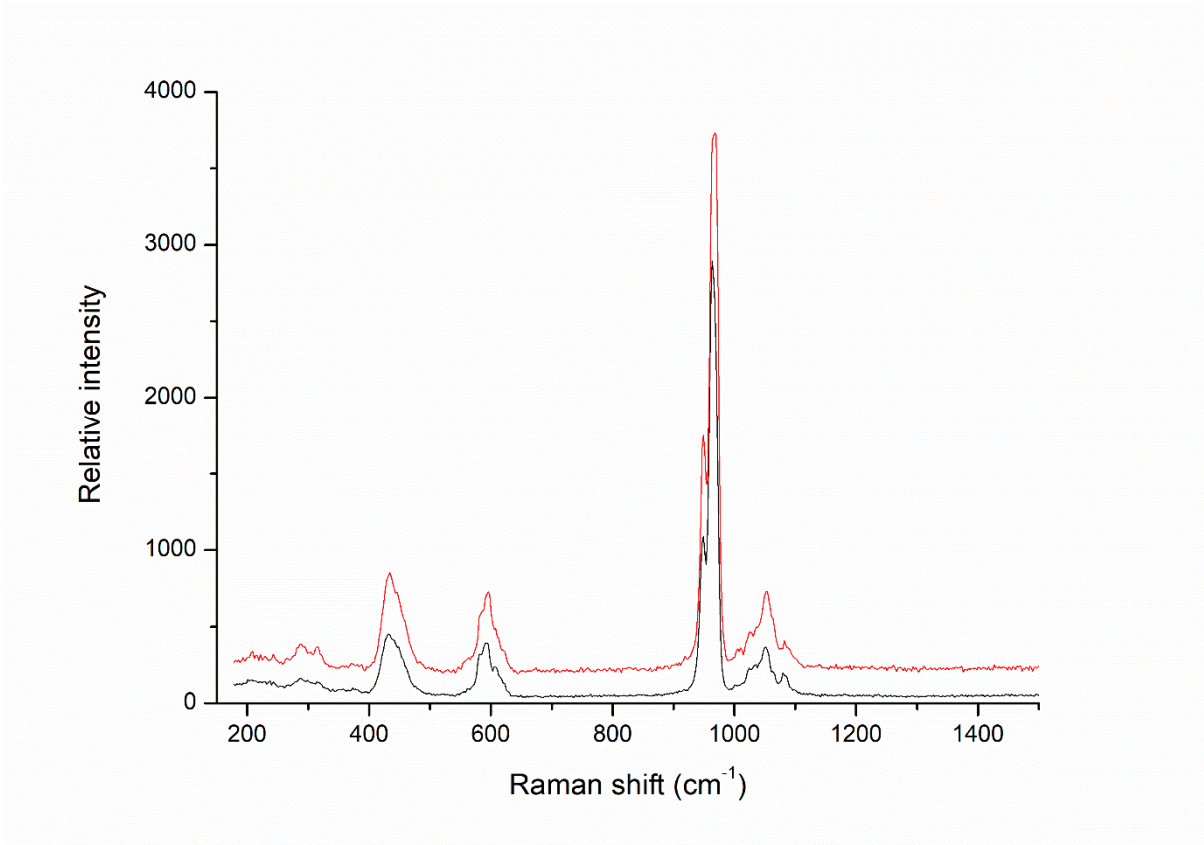

Figure 6. Spectra of a pristine sample (black) and an irradiated sample under air (red).

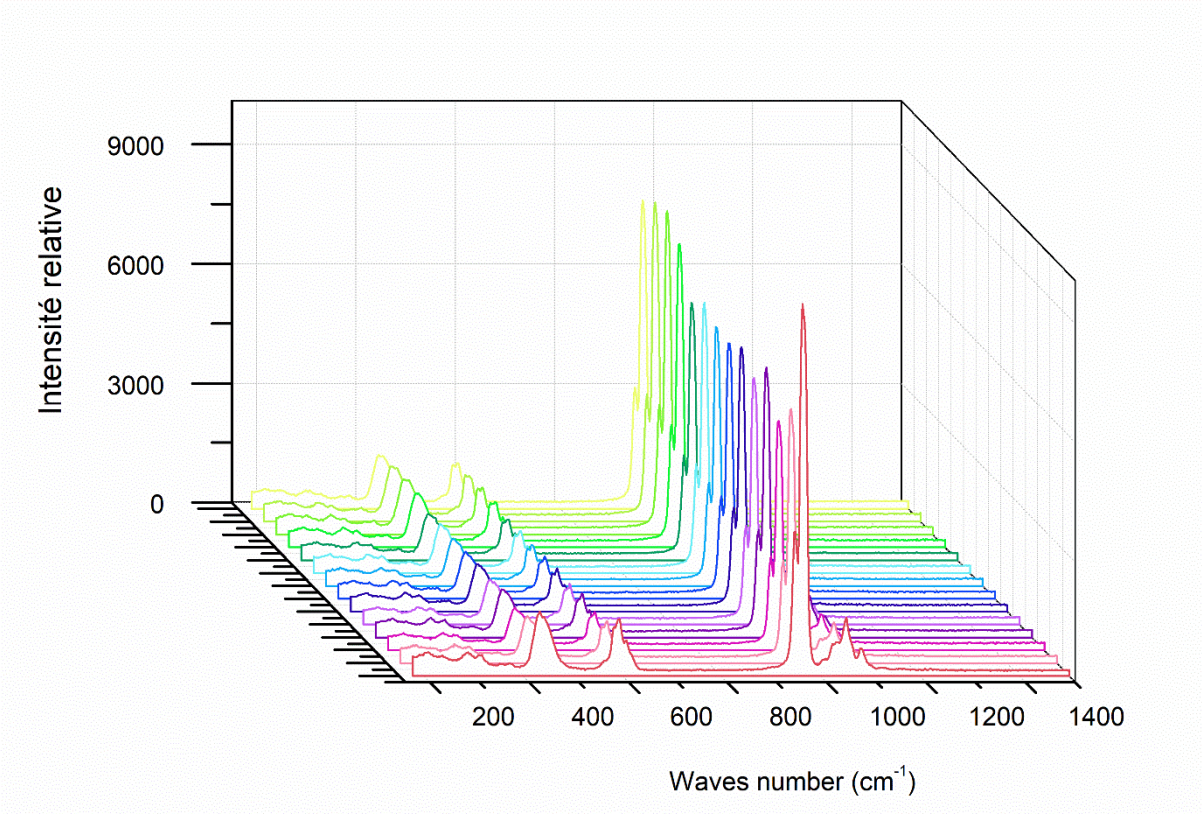

Figure 7. Raman spectra of the realized kinetic on a pristine sample (yellow spectrum at the back = initial time).

3.6. XPS

XPS spectra O 1s, C 1s, Ca 2p and P 2p binding are identical for pristine, EB irradiated in air atmosphere and EB irradiated in N_2 gas atmosphere (Figure 8). Ca/P ratio of pristine, EB irradiated in air atmosphere and EB irradiated in N_2 gas atmosphere are also identical (table 4). Darker areas (Figure 3, B2 and B4) are too small to be detected by XPS analysis.

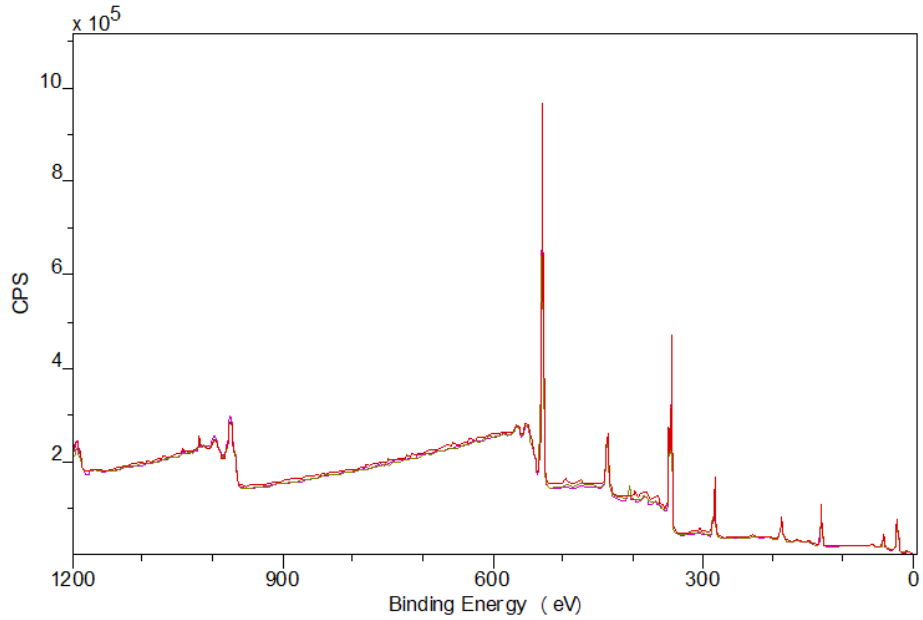

Figure 8. Superimposed XPS spectra of pristine, EB irradiated in air and EB irradiated in gas atmosphere samples.

	Sample	Pristine	Irradiated under air	Irradiated under N_2
Position	O1s	531 / 48.01	531,2 / 49.62	531.1 / 51.74
(eV) / %at of groups	C 1s	284,8 / 27,03	284,8 / 24,15	284,8 / 21,84
	Ca 2p	347,1 /14,46	347,2 / 14,01	347,3 / 14,15
	P 2p	132,9 / 9,27	133,1 / 9,29	133,1 / 9,39
Ca/P		1.6	1.5	1.5

Table 4. Positions (eV), atomic percentage and Ca/P ratio of a pristine sample and both under air and N_2 irradiated samples.

No difference observed between pristine sample and both irradiated under air an N_2 samples. Some carbon pollution was identified on samples by different carbonate groups like C=C, C=O and C-OH liaisons.

4. Discussion

The main results described in this paper are:

- EB induced time limited modification of the wetting property of dry HAP samples;
- Gas atmosphere dependence of EB irradiated grain morphology;

- Dependence of the wetting properties with water saturation for both pristine and EB irradiated samples.

For the first point, It must be noted that – at the dry state, for all characterization techniques used - except for the contact angle, no difference is observed between the pristine ad the irradiated samples which indicates that the irradiation process modifies solely modifies the surface elements related to the wetting properties and not those detected by the Tof SIMS and XPS spectrometry.

Important differences are observed with the previous work of Aronov *et al.* [20,21] both in terms of behavior as we observe an increase of hydrophily while these authors describe opposed the opposite effect and of our previous work carried out on human tooth enamel and dentin [24].

The most likely explanations for this difference is probably the large difference in irradiation conditions (voltage (accelerating voltage: 150keV vs 100eV, fluence: $2{,}34x10^{-2}$ $mC.cm^{-2}$ vs $100\mu C.cm^{-2}$, fluence rate: $2.72x10^{-2}$ $mA.cm^{-2}$ vs $100nA.cm^{-2}$) and also the difference in atmospheric conditions as Aronov *et al.* [20,21] have worked in 10^{-7} Torr vacuum while the present work is carried out in N_2 and in air atmospheres.

Different grain morphologies are observed when the EB irradiation is carried out in air and in N_2 gas atmospheres. This indicates a coupling between the EB irradiation and the ambient gas atmosphere.

Although the voltage used in the present work (150kV) is similar to the one used in the electron microscope (150-400kV), the fluence and fluence rate of the two experimental setups are very different which might explain the absence of amorphization and of CaO grains in the present work.

It is also possible that the electric charge inbalance induced by the electron beam induced by the results in surface and subsurface reconstruction [4,6]. The surface being further modified by surface adhesion [25] which would explain the time limitation of the effect.

We confirm that contact angles reach a plateau with increased water saturation. This shows that the wetting properties of dry HA are not like the ones of water saturated HA. Hydroxyapatite (HA) surfaces exposed, at room temperature, to various aqueous media of different compositions (distilled water, saline solution, cell culture media, saturated HA solution) show an important decrease of the Ca/P atomic ratio of the surface layer was seen on all exposed surfaces, reaching 1, the Ca/P ratio of dicalcium phosphate dihydrate (DCPD) for the uppermost surface layer. Furthermore, $HP0^{2-}$ ions have been observed by XPS and IR by

Amrah-Bouali *et al.* [26]. Furthermore, the combined effect of water and $HPO4^{2-}$- ion on HA lattice expansion has been clearly established by Elliott [27].

This bears some importance for the understanding of the properties of immersed HA as chemical functionalisation processes are performed in a wet state.

5. Conclusion

In the present work we have investigated the effect of EB irradiation on the surface properties of HA ceramics. Three main results are obtained for the irradiation conditions used: 1) time limited modification of the wetting properties of EB irradiated samples, 2) water saturation dependence of contact angles for pristine and EB irradiated samples, 3) gas atmosphere grain morphology dependence of EB irradiated samples. The results constitute the basic information for future developments of EB controlled functionalization of HAP. However, the dependence of HAP damage (or modification) on the irradiation conditions [7,13] must be considered. It cannot be excluded that different effects could be observed under different irradiation conditions. However, the results presented are important for the understanding of the effect of EB surface modification of HA surfaces and for the development EB induced functionalisation of HA bioceramic surfaces.

Acknowledgments

We are grateful to Nicolas NUNS for Tof-SIMS analysis, Ahmed ADDAD and Alexandre FADEL for the help for SEM analysis, Guillaume PENEL and Guillaume FALGAYRAC for Raman analysis and also Pardis SIMON for XPS analysis.

References

[1] Kleebe, H.-J., Brès, E.F., Bernarche-Assolant, D. and Ziegler, G. (1997). High-Resolution Electron Microscopy and Convergent Beam Electron Diffraction Studies of Sintered Undoped Hydroxyapatite. J. Amer. Ceram. Soc. **80**, pp. 37-44.

[2] Dorozhkin, S.V. (2015). Calcium orthophosphate bioceramics. Ceramics International. **41**, pp 13913-13966.

[3] Prakasam, M., Locs, J., Salma-Ancane, K., Loca, D., Largeteau, A. and Berzina-Cimdina, L. (2015). Fabrication, Properties and Applications of Dense Hydroxyapatite: A Review. J. Fonct. Biomater. **6**, pp 1099-1140.

[4] Brès, E.F and Hutchison, J.L. (2002). Observation of the surface structure of biological calcium phosphate apatite crystals from human tooth enamel. Journal of Biomedical Materials Research. Part B: Applied Biomaterials. **63**, pp 433-440.

[5] Tasker, P.W. (1979). The stability of ionic crystal surfaces. Journal of Physics C: Solid State Physics. **12**, pp 4977-4984.

[6] Damia, C., Marchat, D., Lemoine, C., Douard, N., Chaleix, V., Sol, V., Larochette, N., Logeart-Avramoglou, D., Brie, J. and Champion, E. (2019). Functionalization of phosphocalcic bioceramics for bone repair applications. Materials Science and Engineering: C. **95**, pp 343-354.

[7] Eddisford, P., Brown and A. Brydson, R. (2007). Identifying and quantifying the mechanism of electron beam induced damage and recovery in hydroxyapatite. J. of Phys.: Conf. Series. **126**.

[8] Senger, B., Brès, E.F., Hutchison, J.L., Voegel, J.-C. and Frank, R.M. (1991). Ballistic damages induced by electrons in hydroxyapatite. Philosophical Mag. A. **65**.

[9] Reyes-Gasga, J. and Garcia-Garcia, R. (2002). Analysis of the electron-beam radiation damage of TEM samples in the acceleration energy range from 0.1 to 2 MeV using the standard theory for fast electrons. Rad. Phys. and Chem. **64**, pp 359-367.

[10] Nelson, D.G.A., McLean, J.D and Sanders, J.V. (1982). High-resolution electron microscopy of electron irradiation damage in apatite. Rad. Effects. **68**, pp 51-56.

[11] Meldrum, A., Wang, L.M. and Ewing, R.C. (1997). Electron-irradiation-induced phase segregation in crystalline and amorphous apatite: A TEM study. American Mineralogist. **82**, pp 858-869.

[12] Reyes-Garcia, J., Garcia-Garcia, R. and Brès., E. (2009). Electron beam interaction, damage, and reconstruction of hydroxyapatite. Physica B: Condensed Matter. **404**, pp 1867-1873.

[13] Brès, E.F., Reyes-Gasga, J., Rey, C. and Michel, J. (2014). Probe size study of apatite irradiation in stem. The European Phys. J.-Applied Phys. **67**.

[14] Aoba, T., Takahashi, J., Yagi, T., Okazaki, M. and Moriwaki, Y. (1978). High-Voltage Electron Microscopic Study of Dislocations in Hydroxyapatite. J. of Dental Research. **57**.

[15] Reimer, L. (1984). Transmission Electron Microscopy. Springer Series in Optical Sciences.

[16] Nelson, D.G.A. and McLean, J.D. (1984). High-resolution electron microscopy of octacalcium phosphate and its hydrolysis products. Calcified Tissue International. **36**, pp 219-232.

[17] Zhu, H., Kai, Z., Dagang, G., Hang, Z., Sen, Y. and Kewei, X. (2020). *Engineering microstructure of hydroxyapatite by electron beam irradiation to induce controllable in vitro degradation*. Applied Surface Science. In the press.

[18] Brès, E.F., Duhoo, T., Leroy, N. and Lemaitre, J. (2005). Evidence of a transient phase during the hydrolysis of calcium-deficient hydroxyapatite. Zeitschrift für Metallkunde. **96**, pp 503-506.

[19] Aronov, D., Rosen, R., Ron, E.Z. and Rosenman, G. (2006). Tunable hydroxyapatite wettability: Effect on adhesion of biological molecules. Process Biochemistry. **41**, pp 2367-2372. [20] Aronov, D., Molotskii, M. and Rosenman, G. (2007). Charge induced wettability modification. Applied Phys. Letters. **90**.

[21] Aronov, D., Molotskii, M. and Rosenman, G. (2007). Electron-induced wettability modification. Phys. Review B. **76**.

[22] Aronov, D., Karlov, A. and Rosenman, G. (2007). Hydroxyapatite nanoceramics: Basic physical properties and biointerface modification. J. of The European Ceramic Society. **27**, pp 4181-4186.

[23] Aronov, D., Rosen, R., Ron, E.Z. and Rosenman, G. (2008). Electron induced surface modification of hydroxyapatite-coated implant. Surface and Coatings Technology. **202**, pp 2093-2102.

[24] Tiznado-Orozco, G.E., Reyes-Gasga, J., Elefterie, F., Beyens, C., Maschke, U. and Brès. E.F. (2015). *Wettability modification of human tooth surface by water and UV and electron-beam radiation.* Materials Science and Engineering: C. **57**, pp 133-146.

[25] Leeuw, N.H., Mkhonto, D., Richard, C. and Catlow, A. (2003). A Computer Modelling Study of the Adhesion of Apatite Thin Films on Silicate Surfaces, J. Phys. Chem. B. **107**, pp 1-3. [26] Amrah-Bouali, S., Rey, C., Lebugle, A. and Bernache, D. (1994). Surface modifications of hydroxyapatite ceramics in aqueous media. Biomaterials. **15**, pp 269-272.

[27] Elliott, JC. (1994) Structure and chemistry of the apatites and other calcium orthophosphates. Studies I inorganic chemistry 18. Elsevier Amsterdam 152p.

Table of figures